ELSEVIER

Physica D 95 (1996) 35–49

PHYSICA D

Self-consistent simulation studies of non-linear electron-whistler wave–particle interactions

P.E. Devine, S.C. Chapman *

Space and Astrophysics Group, University of Warwick, Coventry, CV4 7AL UK

Received 20 September 1995; revised 6 February 1996; accepted 9 February 1996
Communicated by J.D. Meiss

Abstract

We present results from self-consistent one-dimensional electromagnetic particle-in-cell simulation studies of non-linear electron-whistler wave–particle interactions. In contrast to analytical treatments that assume a constant amplitude, monochromatic wave field, effects on the wave fields due to an evolving electron distribution are self-consistently represented in our simulations (over a wide frequency range from $0.04\omega_{ce}$ to $\sim 100\omega_{ce}$). We analyse the phase space trajectories of the entire set of simulation electrons (many thousands) through application of the delay-coordinate technique. This enables us to establish the trapping frequencies of electrons directly from the trajectories. Additional details in the phase space structure and dynamical changes in the properties of the trajectories are also obtained. Results from two different simulations, in which the wave spectrum is eventually dominated by a single whistler wave mode of relatively large amplitude ($B_w/B_0 \sim 0.2-0.3$), show: (i) the phase space trapping of large numbers of simulation electrons (thousands) with characteristic frequencies around the expected primary trapping resonance frequency estimated from the observed wave amplitude; (ii) more than one strong characteristic frequency component in trapped electron phase space motion; (iii) the dynamics of the trapped process is time dependent, there being an evolutionary shift in time of trapped electron phase space trajectories towards lower characteristic frequencies. We suspect that (ii) is due to the presence of higher order trapping resonances under the relatively large wave amplitude, whilst (iii) is not explained by time independent analytical treatments that neglect the effects of particles on the wave field.

1. Introduction

A great deal of work has addressed the interaction of a monochromatic electron-whistler wave and an energetic resonant electron(s) – such an interaction is thought to be essential in the generation of VLF triggered emissions in the earth's magnetosphere (see the review of [1]). Large amplitude wave–particle interactions are also expected to have fusion device and astrophysical applications [2].

In a system comprising a single charged particle interacting with a monochromatic, constant amplitude wave, it can be shown (e.g. in the case of an electrostatic wave in a constant magnetic field [3]), that a particle may exhibit trapped behaviour, so that in the reference frame of the wave the trapped particle Hamiltonian (to first order in the wave field) describes closed (elliptical) orbits which are a precession about the resonance point in phase space. Retaining higher orders of perturbation in the Hamiltonian generates a self-similar fine scale structure in the phase space orbits, such that trapping is also possible at higher order

* Corresponding author.

PII S0167-2789(96)00057-7

resonances. Such descriptions are non-self-consistent, neglecting for example the effect of trapped particles on the wave field. There have been previous attempts in retaining such effects, such as treating the wave field and trapped particle current in a linear approximation (e.g. [4]). When a completely self-consistent consideration of wave–particle interaction effects on both the wave fields and the electron distribution is desired, appropriate numerical simulations are extremely valuable.

A variety of numerical simulation work, relevant to the nonlinear electron-whistler trapping process, has been performed (see [1]). None have looked at the process in detail by extracting the frequency information present in the entire set of simulation electron trajectories, and the possibility of higher order trapping resonances was never considered. In this paper, we analyse the frequency information present in the velocity space trajectories of electrons (many thousands) that are a representative sample of phase space (both resonant and non-resonant regions of phase space) in a pair of self-consistent one-dimensional (1-D) electromagnetic particle-in-cell (EM PIC) simulations in different regimes. The trajectory time series are reduced by application of the delay-coordinate technique (see, for example [5,6]) enabling us to establish the trapping frequencies of electrons and examine more detailed phase space structure and dynamical changes in the properties of the trajectories. In this way, the studies provide a unique understanding of the non-linear electron-whistler wave–particle interaction.

2. Electron equations of motion in a monochromatic whistler-wave

Assuming a single monochromatic electron whistler mode wave propagating along a background magnetic field $\boldsymbol{B}_0$, with a constant magnetic amplitude $B_w \ll B_0$ (effectively only retaining terms up to first order in the wave field in the perturbed electron Hamiltonian, i.e. $H = H_0 + \epsilon H_1$, where $\epsilon \sim B_w/B_0$ is the expansion parameter of H), it can be shown (e.g. [4]) that some electrons may be 'trapped' on closed phase space orbits around the parallel velocity $v_{\parallel res}$ for cyclotron resonance with the wave (henceforth referred to as the primary trapping resonance), where $v_{\parallel_{res}} = (\omega - \omega_{ce})/k$, and the electron gyrofrequency $\omega_{ce} = eB_0/m_e$. The characteristic frequency of a trapped electron's motion about $v_{\parallel res}$ is the primary trapping frequency, given by

$$\overline{\omega} = \left(\frac{kev_\perp B_w}{m_e}\right)^{\frac{1}{2}}, \tag{1}$$

where k is the wave number, $v_\perp$ the perpendicular electron speed at resonance. Trapped electrons deviate in $v_\parallel$ by at most $\Delta v_\parallel \approx \pm 2^{1/2}\overline{\omega}/k$ from $v_{\parallel res}$ [4].

The assumption $B_w/B_0 \ll 1$ neglects higher than first order wave field effects in the particle equations of phase space motion. If such effects are retained, such as in the general framework single particle, single wave treatment of [3] (note that the interaction considered therein is electron-Langmuir wave, and not electron-whistler), higher order, e.g. secondary and so on, trapping resonances appear within the primary trapping region.

All model wave field treatments assuming constant B_w (including [3]) are non self-consistent, neglecting the effect of particles on the wave field. When a significant fraction of electrons are trapped, phase bunching may occur around a relative particle-wave gyrophase of 180°, representing a so-called 'nonlinear resonant current'. This current will modify the wave fields (see [1]). Important questions to consider are as follows. Does primary trapping exist around $\overline{\omega}$ in a self-consistently evolving system containing a relatively large amplitude whistler wave ($B_w/B_0 \sim 0.2-0.3$ in the simulations presented here)? Do higher order resonances exist under such conditions? Is the phase space structure around resonance stable as assumed in time independent treatments? Under typical conditions for whistler wave growth due to an electron distribution function which is initially anisotropic in velocity space, are the resonant regions of phase space accessible to the particles which are initially not trapped? There have been previous simulation investigations into the trapping process of relevance to the first of these questions (e.g. [7]). However, no detailed analysis of all electron trajectories was

undertaken in such studies, and the other questions were not considered. In an attempt to address these questions, we investigate electron trajectories in various regions of phase space in self-consistent simulations, identify the characteristic frequencies of phase space motion, and look for possible signatures of the various trapping resonances (primary and secondary).

3. Simulation studies

Simulations of the electron-whistler mode instability have been made in 1-D and (previously) 2-D using an EM PIC simulation code (see [8] for details). The simulations presented here are the 1-D studies 1 and 2 contained therein, with run times extended to 25 and 40 electron gyroperiods, respectively. In each, a spatially uniform, energetic electron species with an anisotropic bi-Maxwellian velocity distribution function was initialised (represented by 256 particles per simulation grid cell). A fixed ion background ensured overall charge neutrality. The studies shared an initial electron distribution temperature ratio of $T_\perp/T_\parallel \approx 4$ ($T_{\perp,\parallel}$ being the temperatures perpendicular and parallel to the initially uniform background magnetic field $\boldsymbol{B}_0 = B_0\hat{\boldsymbol{x}}$) and plasma frequency $\omega_{pe} = 10^5$ rad s^{-1}. The ratio $\beta_\parallel = (n_e k B T_\parallel)/(B_0^2/2\mu_0)$ was varied in the two studies ($\beta_\parallel = 0.14$ in study 1, and 0.45 in study 2). The initial electron distribution $f(v)$ is unstable to the growth of whistler waves (see [8]), and in both studies the wave spectrum is eventually dominated by a single, large amplitude, electron-whistler mode (actually two waves of identical $|k|$ and opposite $\hat{k}$, since $f(v)$ is non-beam like).

Due to our use of periodic boundary conditions, only waves that fit an integral number of times into the simulation box length (L_x) are resolved, resulting in a discrete set of wave numbers $k_x = 2\pi n_x/L_x$ where $n = 0, \pm1, \pm2 \ldots$. We used 128 simulation grid cells, each of size $\Delta x = \lambda_D$ (Debye length) to avoid possible numerical instability [9], giving $|k_x|_{min} = 2\pi/128\lambda D$ and $|k_x|_{max} = \pi/\lambda D$. Electrostatic and electromagnetic effects are resolved over a frequency range from $\omega_{min} = 0.04\omega_{ce}$ to $\omega_{max} = 80\omega_{ce}$ (study 1), $\omega_{min} = 0.025\omega_{ce}$ to $\omega_{max} = 370\omega_{ce}$ (study 2). The maximum phase speed represented $\omega_{max}/k_{max} = 1.7c$ (study 1) and $1.74c$ (study 2) (based on $\lambda D(T_\parallel)$) so that the simulation bandwidth just includes $kc/\omega = 1$; the regime for (relativistic) auto-resonance [10]. The initial anisotropic electron distribution is however, chosen to be unstable to modes of much lower ω, k than these [8] and we shall see that resonance occurs with modes of much larger kc/ω so that relativistic effect are weak.

Importantly, we perform and compare the results from two simulation studies, in which the trapping frequency $\overline{\omega}$ scales differently relative to the real wave frequency ω. This allows us to unambiguously distinguish the $\overline{\omega}$ (determined from the particle trajectories) from the possible effect of waves which are unrelated to the trapping process.

4. Results of simulations

4.1. One-dimensional study 1

Fig. 1 shows the growth of magnetic energy in the linearly predicted growth wave modes containing most energy ($K_x = 4, 5$ and 6), relative to the total system magnetic wave energy ('Total'), during the 1-D study 1 (see [8] for details). Note that we label wave modes by the convenient dimensionless wave numbers $K_x = (1 + |k_x|L_x/2\pi)\,\mathrm{sgn}(k_x)$, as used in Fig. 1.

Units of time in Fig. 1 are in simulation time steps Δt, i.e. $\tilde{t} = t/\Delta t$ is used as the time coordinate. The electron plasma period τ_{pe} and gyroperiod τ_{ce} correspond to 80 and 160 Δt respectively, and the run time was $4000\Delta t$ ($25\tau_{ce}$). Two roughly distinct time intervals are identified:- (i) $\tilde{t} < 2000$ (early), during which energy resides in several growth modes at a comparable level; (ii) $\tilde{t} > 2000$ (late), during which the wave spectrum is dominated (>95% of total) by wave mode $K_x = 4$ (this energy being shared roughly equally (within noise levels) between the two oppositely propagating wave modes $K_x = \pm4$; the effects of this on electron dynamics are considered in more detail later). Any trapping of electrons with this mode will be subrelativistic as $k_4 c/\omega_4 \approx 5.6$ (auto-resonance requires $kc/\omega = 1$).

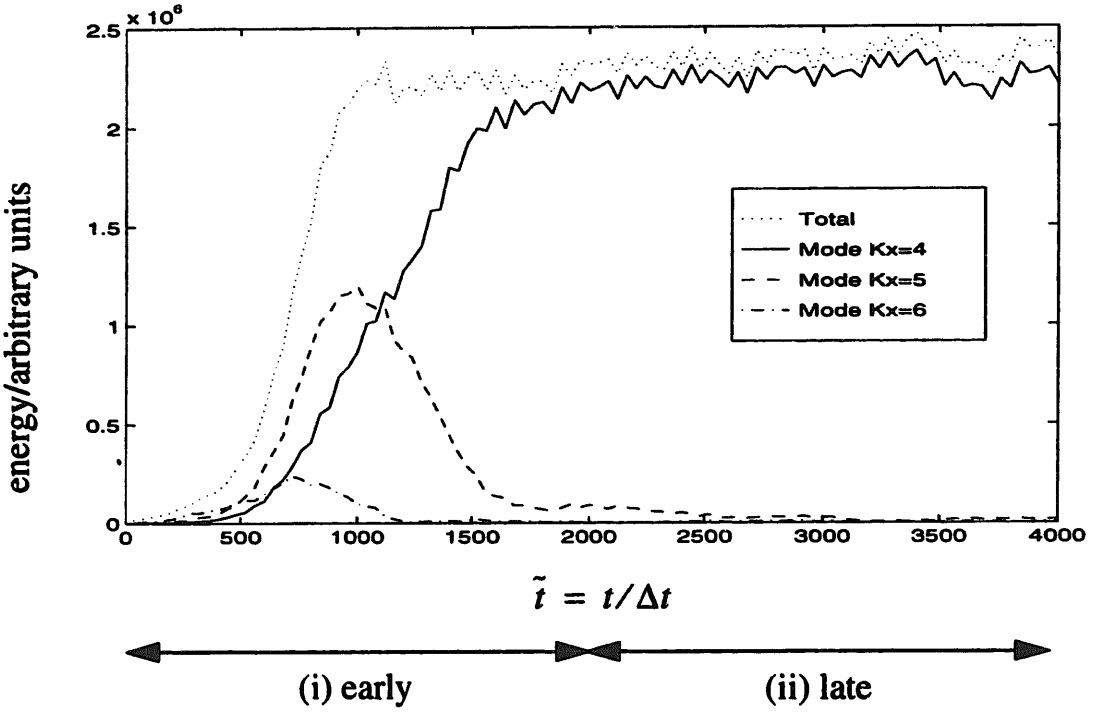

Fig. 1. Magnetic energy in simulation wave modes $K_x = 4$–6 during 1-D study 1.

An estimated mode $K_x = 4$ primary electron trapping frequency during $\tilde{t} > 2000$, using (1) with a typical $\langle v_\perp \rangle = 1.5 \times 10^8\,\mathrm{m\,s^{-1}}$ and the observed mode 4 wave amplitude at $\tilde{t} \approx 3000$ ($B_w/B_0 \approx 0.2$), is $\overline{\omega} \approx 0.36\omega_{ce}$. This corresponds to an estimated trapping period of $\overline{\tau} = 2\pi/\overline{\omega} = 440\Delta t$. Fluctuations in $\overline{\omega}$ (at a fixed $v_\perp$), due to fluctuations in B_w during $\tilde{t} > 2000$ (see Fig. 1) are less than 5%, and are not expected to be important. However, as $\overline{\omega}$ is $v_\perp$-dependent, an estimated $\overline{\tau}$ range, that accounts for both the variation in $v_\perp$ of a single trapped electron along its phase space orbit, and different $v_\perp$ for different trapped electrons, is appropriate. We calculate $\overline{\tau} = 360-620\Delta t$ for electrons within $v_\perp = 1 \times 10^8 - 2 \times 10^8\,\mathrm{m\,s^{-1}}$ (relativistic mass variations have been ignored, giving only ~5% discrepancy in $\overline{\omega}$). The interval $2000 \leq \tilde{t} < 4000$ is therefore expected to contain several $\overline{\tau}$ for the majority of trapped electrons.

The linearly predicted mode 4 growth and real frequencies [8] are $\gamma_4 \approx 0.02\omega_{ce}$ and $\omega_4 \approx 0.4\omega_{ce}$ respectively, so that trapping effects are fast (non-adiabatic) with respect to gyromotion, occurring on a timescale $\sim\tau_{ce}$ (adiabatic simulations with a low ratio of $\overline{\omega}/\omega$ will require a much longer run time in order to observe trapping effects). For a given electron, $\overline{\tau}$ is estimated at exact resonance (e.g., [11]), i.e. its minimum value, so that effects associated with the observed trapping period $\overline{\tau}$ and mode 4 wave period $\tau_4 = 2\pi/\omega_4$ will be seen to be distinguishable, even though $\overline{\tau}$ and τ_4 differ by only ~10%. Trapping effects are not expected to be important for other simulation wave modes during $\tilde{t} > 2000$, since their amplitudes are generally too low (see, for example, $K_x = 5, 6$ in Fig. 1).

The $v_\parallel$ vs. time of nine electron orbits initially in the region of $v_\parallel \approx 5.8 \times 10^7\,\mathrm{m\,s^{-1}}$ are shown in Fig. 2. Particularly after $\tilde{t} > 2000$, these are strongly suggestive of large excursions in $v_\parallel$ with some periodicity on more than one characteristic time scale. To investigate the electron dynamics occurring in the entire simulation, an analysis of the frequency information in all of the electron trajectories is required. This is achieved here by extracting the times at which trajectories cross a specified phase space plane of constant $v_\parallel = v_{\parallel c}$ (relative to the initial geometry of B_0), giving a much reduced time series. For a given $v_{\parallel c}$, a delay-coordinate plot is then constructed by plotting the successive full oscillation periods for all electrons crossing $v_{\parallel c}$ on a

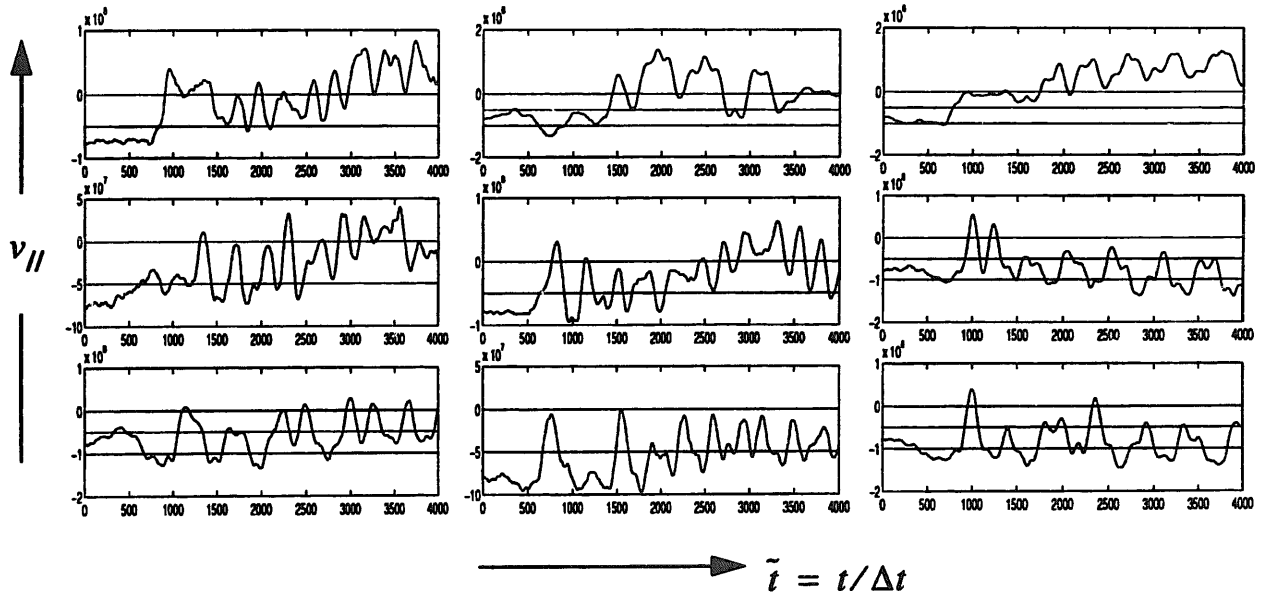

Fig. 2. Velocity trajectories of nine selected electrons from 1-D study 1. The three chosen velocity surfaces for delay coordinate plots are also shown as horizontal lines.

scatter plot as discussed further below. Three separate $v_{\|c}$ were chosen, and the plots were constructed for each of these, separately for the two chosen time intervals. As indicated by the horizontal lines in Fig. 2, surfaces $v_{\|c} = 0, -5\times10^7, -1\times10^8\,\mathrm{m\,s^{-1}}$ were chosen. Fig. 3 illustrates the phase space geometry of these relative to the parallel cyclotron resonance velocities ($v_{\|res}$) for the wave modes of Fig. 1. The estimated width of the mode 4 trapping region shown in Fig. 3 ($\Delta v_\| \approx 1\times10^8\,\mathrm{m\,s^{-1}}$) is based on a value of $\langle v_\perp\rangle \approx 1.5\times10^8\,\mathrm{m\,s^{-1}}$. Based on their proximity to the dominant mode 4 resonant velocity and trapping region, the three surfaces $v_{\|c} = -1\times10^8, -5\times10^7, 0\,\mathrm{m\,s^{-1}}$ are henceforth labelled 'near resonance', 'off resonance', and 'far off resonance' respectively. Electron trapping effects are expected to be seen chiefly in crossings of the 'near resonance' and to a lesser extent in 'off resonance' surfaces, but are not expected to be important in the 'far off resonance' surface.

As highlighted earlier, the mode 4 energy is shared equally (within noise levels) between the two modes $K_x = \pm4$. The linearly predicted cyclotron resonance velocities for these two modes are $v_{\|res} = \mp1.3\times10^8\,\mathrm{m\,s^{-1}}$ respectively [8]. Since $\Delta v_\| \approx 10^8\,\mathrm{m\,s^{-1}}$ typically (see above), there is expected to be little (or no) overlap of the trapping regions for $K_x = 4$ and -4 (see Fig. 3), i.e. any trapping of electrons in $v_\| < 0$ is due to the single wave mode $K_x = +4$ only (this will be verified later through the delay-coordinate plots).

Separate data sets were formed for each $v_{\|c}$, each containing all the times $t_1, t_2, \ldots$ at which particles cross the surface during the entire simulation (see the examples in Figs. 4 and 5). For each $v_{\|c}$, successive full oscillation periods $\Delta t_n = t_{n+2} - t_n$, $\Delta t_{n+1} = t_{n+4} - t_{n+2}$.., were formed for all particles that crossed the surface. Each pair of successive crossing periods or coordinate pair $(\Delta t_n, \Delta t_{n+1})$ was then allocated to the time interval $\tilde{t} < 2000$ or $\tilde{t} > 2000$ applicable to the time period t_n to t_{n+4} spanned by the crossings.

For a particular data set (i.e. chosen $v_{\|c}$ and time interval), a delay-coordinate plot was formed by plotting the set of (x, y) points $\{\Delta t_{1\ldots N_p-1}, \Delta t_{2\ldots N_p}\}_p$ for all particles that crossed the chosen $v_{\|c}$ (N_p denoting the number of crossing periods for a particle p in the set), i.e. overlaying the plots of many thousands of particles.

Expected signatures in the delay-coordinate plots are as follows. In general, a single characteristic frequency ω in the electron $v_\|(t)$ would yield a single dot on the delay-coordinate plot at $\Delta t_{n+1} = \Delta t_n = 2\pi/\omega$ (see Fig. 4; in this and all subsequent delay-coordinate

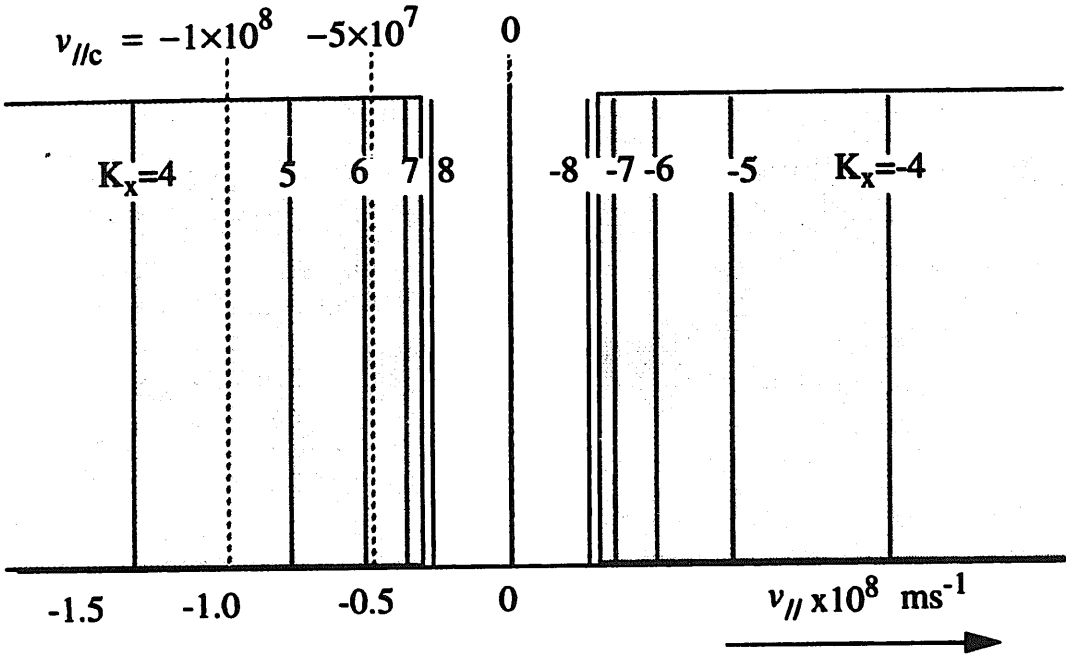

Fig. 3. A phase space picture of the cyclotron resonances and the estimated mode 4 trapping region in 1-D study 1. Solid vertical lines represent linearly predicted cyclotron resonance velocities for the growth modes K_x = 4–8, –4 to –8; dotted vertical lines represent parallel velocity surfaces chosen for delay-coordinate purposes. The shaded area represents the estimated mode 4 trapping region.

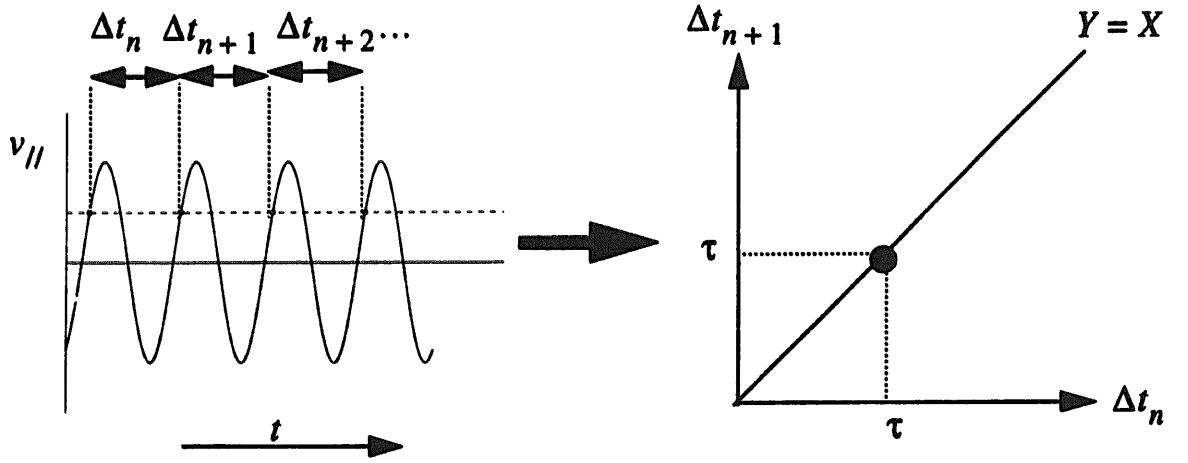

Fig. 4. Periodic electron phase space motion at a single characteristic frequency ω yielding a dot at $\Delta t_{n+1} = \Delta t_n = \tau = 2\pi/\omega$ on the delay-coordinate plot.

plots the line $\Delta t_{n+1} = \Delta t_n$, or $y = x$, is included to highlight periodic motion at a single frequency). Two characteristic frequencies of motion would combine to give two dots symmetrically positioned about $y = x$ at $\Delta t_{n+1} = \tau_2$, $\Delta t_n = \tau_1$ and vice versa (see Fig. 5; see also the trajectories in Fig. 2). Similarly, the presence of multiple characteristic frequencies in the $v_{\|}(t)$ time series would generate a grid of dots on the delay-coordinate plot at the various time periods. For a given $v_{\|c}$, the resulting frequency grid expected to be most evident in the delay-coordinate plot will result from the combination of the dominant characteristic frequencies in trajectories in the region of phase space local to $v_{\|c}$. We expect the possible characteristic frequencies in the simulation system to be: (i) a quantised 'grid' of all wave mode frequencies ω_j present in the simulation. This results from the effects of these modes on electron phase space

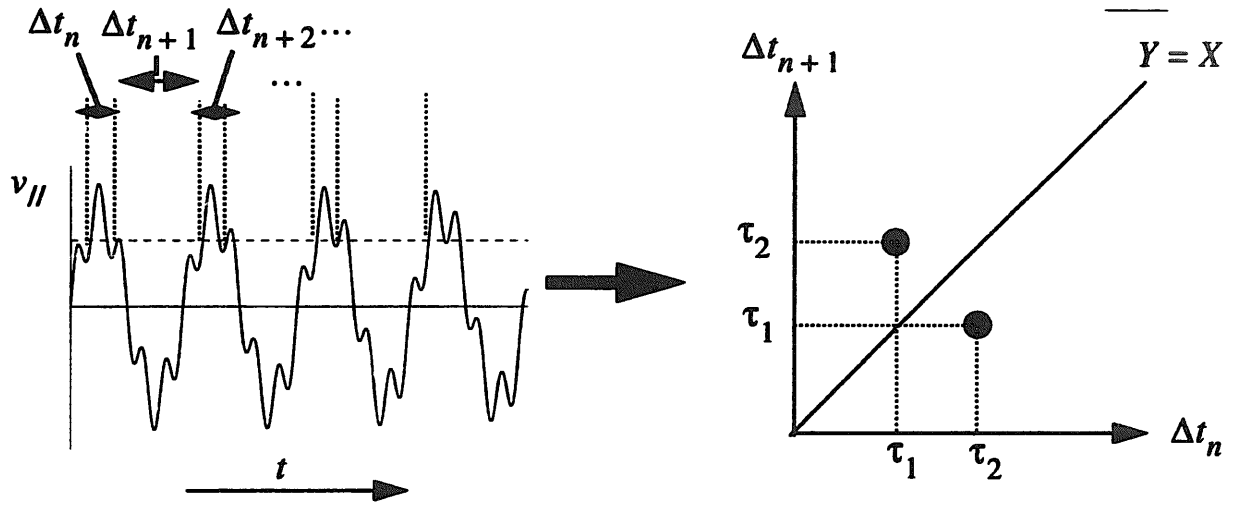

Fig. 5. Electron phase space motion showing two characteristic frequencies ω_1, ω_2. The resulting delay-coordinate plot shows dots at τ_1 and τ_2.

motion (all modes contain at least noise fluctuation level energy during the simulation); (ii) trapping frequencies associated with the dominant mode during the later stages of the simulation; (iii) the electron gyrofrequency ω_{ce} of untrapped electrons with $v_{\|} \approx v_{\|c}$ and significant $v_{\perp}$ (since $v_{\|}$ is defined as along the initial background magnetic field $\boldsymbol{B}_0$, rather than the total magnetic field $\boldsymbol{B}_t$ about which gyromotion occurs, then for sufficiently large $v_{\perp}$, the $v_{\|}(t)$ as defined acquires a component of electron gyromotion). In the $v_{\|}(t)$ we then expect: *near resonance* ($v_{\|c} = -1 \times 10^8\,\mathrm{m\,s^{-1}}$), the nearest whistler mode resonance is through the dominant mode 4 (see Fig. 3), and the strongest characteristic frequencies are expected to be: the primary trapping frequency $\bar{\omega}$, the freqencies associated with higher order resonance effects (if such effects are important), and the electron gyrofrequency ω_{ce} (perturbations in $v_{\|}(t)$ due to noise level energy in all other simulation wave modes will in comparison be relatively weak near resonance. *Off resonance* ($v_{\|c} = -5 \times 10^7\mathrm{m\,s^{-1}}$), we again expect the trapping and gyrofrequencies. Also, the effect of noise in other simulation wave modes will be more pronounced (since the trapping effect is weaker and a smaller fraction of the trajectories sampled are trapped off resonance), hence the grid ω_j of simulation wave mode frequencies should also contribute to the overall frequency grid. Finally, *far off resonance* ($v_{\|c} = 0$), trapping effects are expected to be very weak, most trajectories sampled are untrapped, and we expect the ω_j grid to be the strongest set of characteristic frequencies in the delay-coordinate grid (the plane $v_{\|c} = 0$ cuts the peak of the electron distribution, $v_{\|}, v_{\perp} = 0$, hence most trajectories will not display gyromotion signatures).

4.1.1. $v_{\|c} = -10^8\,\mathrm{m\,s^{-1}}$ *crossings (near resonant)*

Fig. 6(A) and (B) contain the delay-coordinate plots for $v_{\|c} = -10^8\,\mathrm{m\,s^{-1}}$ crossings. Note that the axes on the delay-coordinate plots relevant to (A) $\tilde{t} < 2000$, (B) $\tilde{t} > 2000$, respectively correspond to simulation times $\tilde{t} = 0 - 2000$ and $\tilde{t} = 2000 - 4000$, over which the information was obtained. These reveal the following:-

Fig. 6(A) $\tilde{t} < 2000$:- No apparent correlation between subsequent full oscillation periods exists, i.e. no single clear relationship between Δt_{n+1} and Δt_n ($\tau_{pe} = 80$ and $\tau_{ce} = 160$ simulation time steps have been included in Fig. 6(A) for reference). During $\tilde{t} < 2000$, the wave spectrum is strongly non-time stationary, with various wave modes growing, saturating, and decreasing in amplitude, on a time scale less than any individual trapping periods (see Fig. 1). As a result, trapping effects do not occur.

Fig. 6(B) $\tilde{t} > 2000$:- A strong bunching of points around several characteristic periods is now evident. Horizontal/vertical lines in Fig. 6(B) represent τ_{ce} and the mode 4 trapping period $\bar{\tau} = 440$ (the estimated

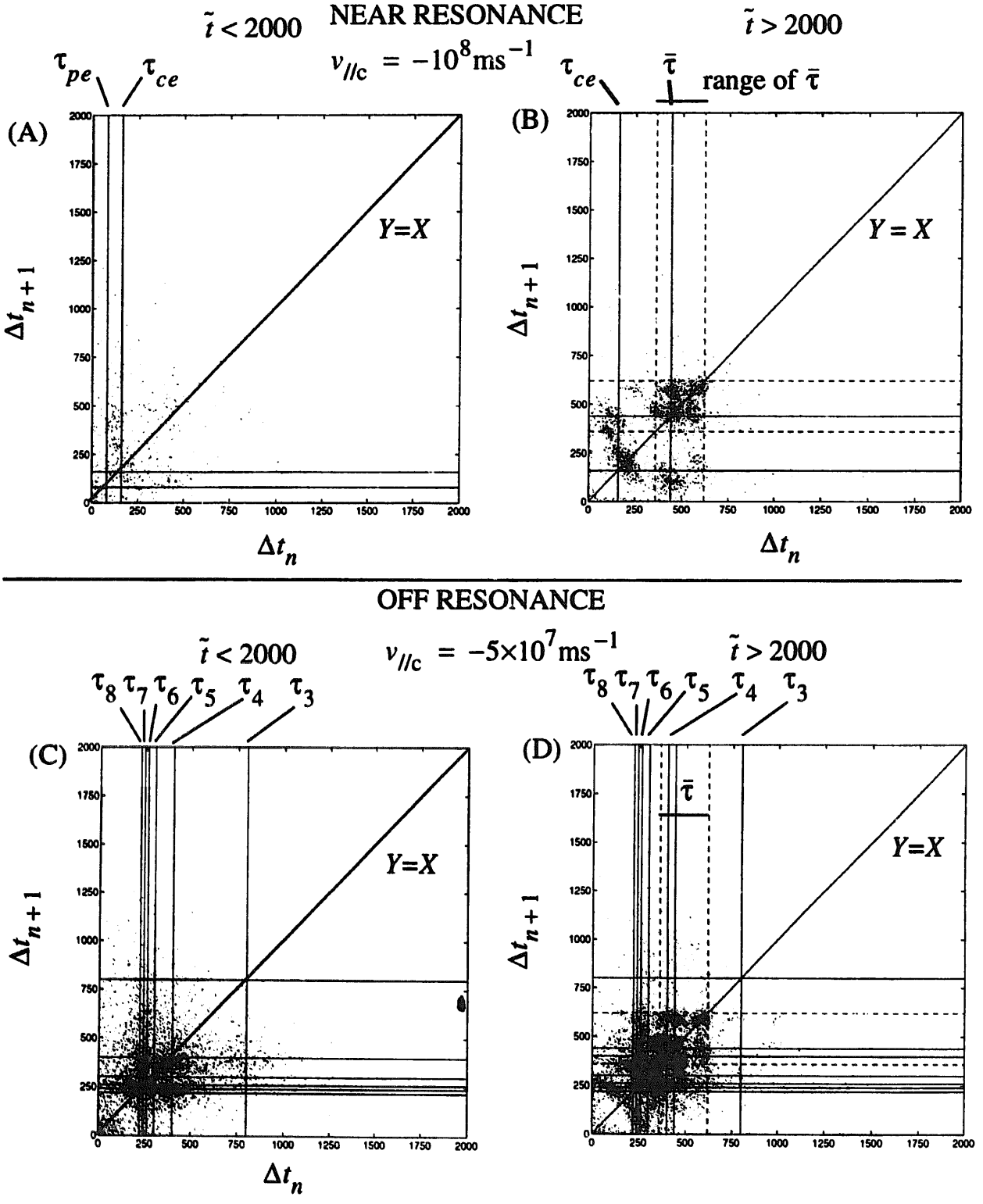

Fig. 6. (A–D) 1D study 1 delay-coordinate plots showing pairs of crossing periods $(\Delta t_n, \Delta t_{n+1})$ of:- (A), (B): $v_{\|c} = -10^8\,\mathrm{m\,s^{-1}}$ during $\tilde{t} < 2000$ and $\tilde{t} > 2000$; (C), (D): $v_{\|c} = -5 \times 10^7\,\mathrm{m\,s^{-1}}$ during $\tilde{t} > 2000$ (E–F) 1D study 1 delay-coordinate plot. Crossings of $v_{\|c} = 0$ during:- (E) $\tilde{t} < 2000$, (F) $\tilde{t} > 2000$.

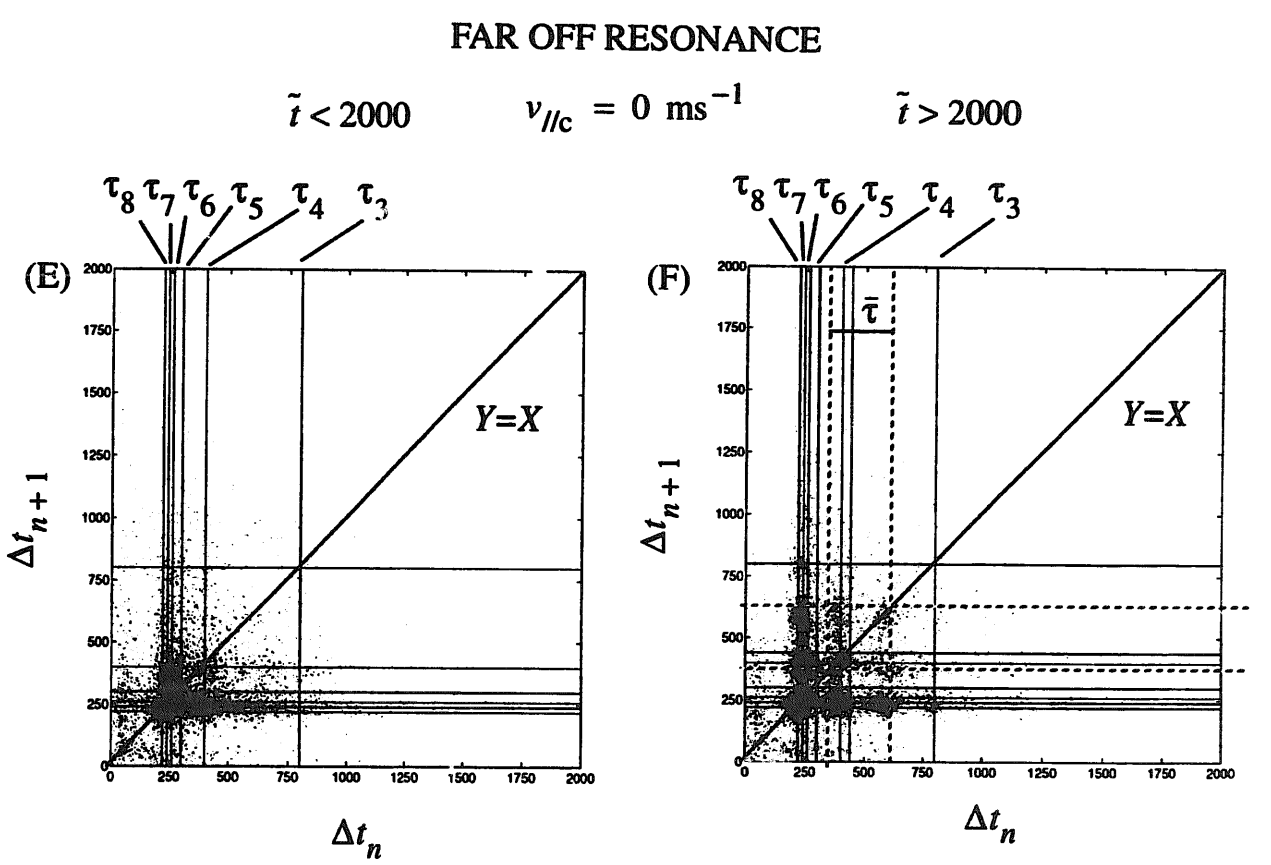

Fig. 6. (continued)

range of $\bar{\tau}$ due to the range of $v_\perp$ in the electron $f(v)$ is represented by the dashed lines at 360, 620 time steps).

One such bunching is around $\sim\tau_{ce}$, implying a significant number of near resonant electrons ($v_\parallel \approx v_{\parallel res}$) are simply undergoing gyromotion rather than trapped motion. As described earlier, provided $v_\perp$ is significant gyromotion effects will appear in the delay-coordinate plot due to a 'tilt' of $v_\parallel$ with respect to the total magnetic field in the system about which gyromotion occurs.

A second characteristic crossing period that may be identified is the primary trapping period $\bar{\tau}$. Around this a cluster of points is evident spanning the estimated range of $\bar{\tau}$. The position of $\bar{\tau}$ at the bottom left of the cluster of points corresponds to the minimum in $\bar{\tau}$ calculated for motion exactly on resonance (from Eq. (1)). Hence, this feature is identified as the trapping of a significant number of electrons (approximately 1600 particles each contribute an average of 2–3 points to Fig. 6(B)). Since there is not a simple spread in the data points around $\bar{\tau}$ and along the line $y = x$, or a stochastic spread about $\bar{\tau}$ and $y = x$, neither a first order ($B_w \ll B_0$) model wave field description (e.g. [4]), nor the combination of a first order description and stochastic (noise like) wave fluctuations, can account for the observed distribution of points at/around $\bar{\tau}$. Instead, there appear to be 4–5 distinguishable clusters of points in the $\bar{\tau}$ range, both on and off $y = x$. This indicates at least two strong characteristic frequencies in the velocity space trajectories of trapped electrons near resonance. The time separation between the centres of the two trapped clusters lying on $y = x$ is approximately 125, with corresponding frequencies $\approx 0.35\omega_{ce}$ and $\approx 0.27\omega_{ce}$ respectively, i.e. a frequency difference $\Delta\bar{\omega} \approx 0.08\omega_{ce}$, approximately 20–25% of the primary trapping frequency $\bar{\omega} \approx 0.36\omega_{ce}$. Note that the mode 4 linearly predicted real frequency ($\omega_4 = 0.4\omega_{ce}$) exceeds $\bar{\omega}$ by $0.04\omega_{ce}$, a difference within a factor $\sim$2 of the observed frequency difference in the trapped population(s). We suspect that this is coincidental, however, since in our second simulation, under a different

ratio of $\overline{\omega}/\omega$ (where ω is the dominant wave mode's real frequency), the frequency difference $|\omega - \overline{\omega}|$ can not possibly account for the structure in the trapped population. A plausible explanation for the observed pattern is the onset of secondary trapping resonances, which will appear at different characteristic frequencies around $\overline{\omega}$. Trapped electron phase space orbits close to higher order resonances may explain the additional strong characteristic frequencies contributing to Fig. 6(B).

Fig. 6(B) also displays an asymmetry about $y = x$ in the distribution of crossing period points at/around $\overline{\tau}$, with a cluster of points with $\Delta t_n < \overline{\tau}$ and $\Delta t_{n+1} > \overline{\tau}$ (just to the left and above $\overline{\tau}$), for which there is a very weak corresponding cluster in the 'mirror region' about $y = x$ (just to the right and below $\overline{\tau}$) instead, a scatter of far fewer points is present in this region (enlarged in Fig. 7). The number of points lying within two equal size square mirror regions $(\Delta t_n, \Delta t_{n+1}) =$ (340–440, 440–540) and (440–540, 340–440), one above and to the left of $\overline{\tau}$, the other below and to the right, are 206 and 106, respectively. The difference (100 points) is larger than $\sqrt{N}/N$ statistical uncertainties in the box occupancies (e.g. $\sqrt{206} \approx 14.4$) by a factor ~7–10. With regards the entire trapped population, the number of points in the square region $\Delta t_n, \Delta t_{n+1} = 300$–$700$ time steps is 1628, 922 of which lie above $y = x$, and 706 below, the difference (216) being $(7\text{–}8)\times\sqrt{N}/N$. Hence, there are more points in the trapped population above $y = x$ than below, the difference being statistically significant.

This implies a net shift in time of electron motion (in $v_{\|}(t)$) towards a longer characteristic period (lower frequency); the trapped electrons in the asymmetric feature in Fig. 6(B) have $\Delta t_{n+1} > \Delta t_n$ more often than $\Delta t_n > \Delta t_{n+1}$. The Δt_{n+1} of this region on the plot is not the largest value of Δt in the cluster of points around $\overline{\tau}$ and presumably then does not correspond to motion close to the separatrix of the trapping region. Note that the mode 4 amplitude slowly increases (by ~10%) during $\tilde{t} > 2000$ (see Fig. 1). However, since $\overline{\omega} \propto \sqrt{B_w}$ (see [1]), an increase in B_w alone would actually imply a gradual increase in $\overline{\omega}$ i.e. decrease in $\overline{\tau}$, although for the small (~10%) variation in B_w, this effect is very weak. This is not consistent with the observed evolution of trapped electron dynamics towards a lower frequency, so that the time dependence in the trapping is not simply accountable for by a slowly evolving wave amplitude. The system of a single electron in a monochromatic wave propagating along uniform constant background magnetic field has two space degrees of freedom (z, where $\dot{z} = v_{\|}$ and ψ, the angle between $-\boldsymbol{B}_w$ and $\boldsymbol{v}_{\perp}$) and if the wave amplitude is time varying, a third degree

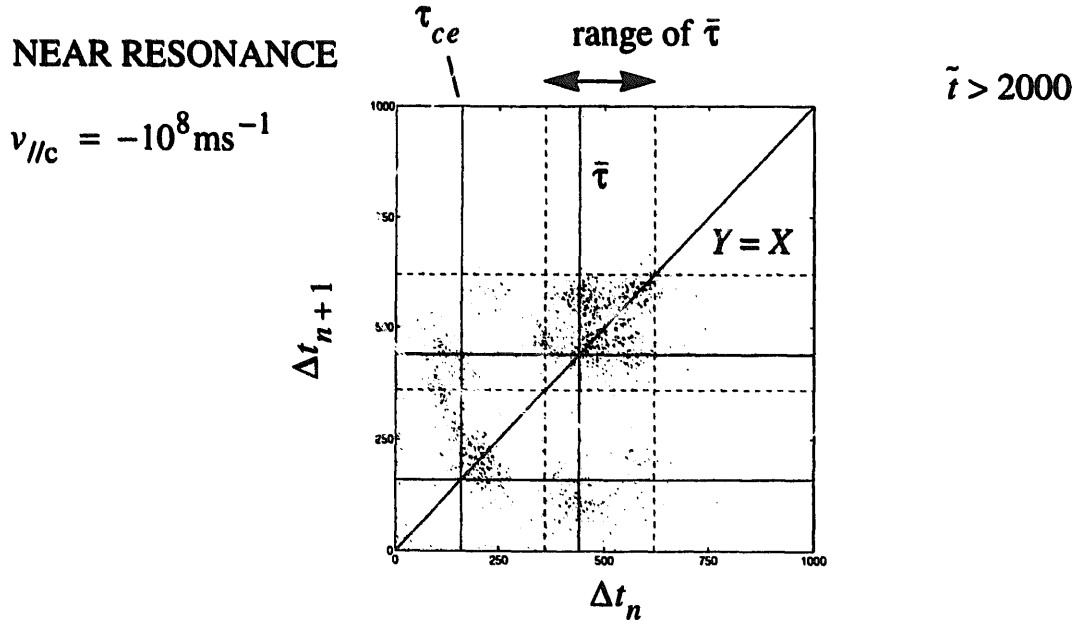

Fig. 7. An enlargement of Fig. 6(B) delay-coordinate plot for $v_{//c} = -10^8\ \mathrm{ms}^{-1}$ crossings during $\tilde{t} > 2000$.

of freedom (effectively t). The time variation in B_w introduces the possibility of Arnold diffusion; an estimate of the rate of diffusion of trapped electron orbits in phase space is given by the variation of the width of the trapping region $\Delta v_\parallel \propto \overline{\omega} \propto \sqrt{B_w}$, again, this is weak. We might also expect Arnold diffusion to evolve the trapping period to a maximum (as trapped electrons move towards the separtrix), which is not the case here.

4.1.2. $v_{\parallel c} = -5 \times 10^7\ \mathrm{m\,s^{-1}}$ crossings (off resonance)

Fig. 6(C) $\tilde{t} < 2000$:- A wide scatter of points spanning the range of individual wave mode periods $\sim \tau_{6-8}$ and $\sim \tau_4$ is evident. The set of lines in Fig. 6(C) represent, in increasing order of wave period (high → low frequency), the grid of linearly predicted whistler wave periods of the simulation modes $K_x = 8, 7, 6, 5, 4, 3$. Only modes up to $K_x = 8$ are shown because adjacent wave periods are very close in value above this (modes up to $K_x = 65$ exist in the simulation).

Fig. 6(D) $\tilde{t} > 2000$:- A grid of characteristic periods of electron phase space motion around $v_{\parallel c} = -5 \times 10^7\ \mathrm{ms^{-1}}$ during $\tilde{t} > 2000$ is observed. This results from the coupling of many characteristic frequencies. As we move the $v_{\parallel c}$ surface further from resonance, we expect the $v_\parallel(t)$ to be more strongly perturbed by the (noise level) fields resident in all wave modes allowed in the simulation. The delay-coordinate plot hence begins to reveal both the signature of oscillations at the mode 4 trapping frequency $\overline{\omega}$ and motion at the other wave mode frequencies (ω_j, e.g. for modes $K_x = 6$–8 included in Fig. 6(D)). The population of trapped electrons within the $\overline{\tau}$ range in Fig. 6(D) displays a pattern that is very similar to that seen near resonance during the same time interval (see Fig. 6(B)). There is, however, an additonal strong bunching of points at the bottom corner of the $\overline{\tau}$ range in Fig. 6(D) that is not present in the near resonance plot. Since the mode 4 trapping region overlaps the mode 5–7 cyclotron resonant regions of velocity space close to the $v_{\parallel c} = -5 \times 10^7\ \mathrm{m\,s^{-1}}$ surface (see Fig. 3), it is possible that off resonance overlap effects complicate the delay-coordinate plot relative to near resonance.

4.1.3. $v_{\parallel c} = 0$ crossings (far off resonance)

Fig. 6(E) $\tilde{t} < 2000$:- As anticipated earlier, we observe a strong bunching of points at the frequencies of individual wave mode periods $K_x = 6, 7, 8$.

Fig. 6(F) $\tilde{t} > 2000$:- There is now no evidence of the trapped population seen near and off resonance. In addition to the cluster of points noted above, the grid of strong characteristic frequencies now includes the mode 4 wave period τ_4 (400 time steps) on the line $y = x$. Coupling of the many characteristic frequencies produces the clusters of points off $y = x$. Finally, there are weak clusters of points in Fig. 6(F) at approximately $(\Delta t_n, \Delta t_{n+1}) = (250, 600)$ and $(600, 250)$. A time period of 600 Δt corresponds roughly to the upper limit of the estimated range in $\overline{\tau}$. We therefore, interpret this as the coupling of wave mode $K_x = 6, 7, 8 \ldots$ frequencies and the characteristic frequency of mode 4 trapped electrons that are closest to the separatrix and have large enough amplitudes of oscillation to reach $v_{\parallel c} = 0$ (as seen in some of the Fig. 2 trajectories, some trapped electrons do have sufficient amplitude to reach $v_{\parallel c} = 0$).

4.2. One-dimensional study 2

Fig. 8 shows the magnetic wave energy in the linearly predicted growth modes containing most energy during 1-D study 2 (τ_{pe}, $\tau_{ce} = 130$ and 740 simulation timesteps respectively). During $\tilde{t} > 10000$, over 95% of the system magnetic wave energy resides in wave mode $K_x = 2$ (shared roughly equally between the two wave modes $K_x = \pm 2$, but this is not expected to be an important consideration in the delay-coordinate plots, for the reasons outlined earlier). Three time intervals of interest are approximately identified, during which the wave spectrum energy:- (i) $\tilde{t} < 5000$ resides in several growth modes, and is then dominated by mode $K_x = 3$; (ii) $5000 \leq \tilde{t} \leq 10000$ shared (unequally but comparably) between two wave modes $K_x = 3$ and 2; (iii) $\tilde{t} > 10000$ dominated by mode $K_x = 2$. Again, resonance with mode 2 will be nonrelativistic since $k_2 c/\omega_2 \approx 15.2$.

Based on the mode 2 amplitude $B_w/B_0 \approx 0.3$ at $\tilde{t} \approx 10000$ (c.f. $B_w/B_0 \approx 0.2$ in study 1), and using (1) with a variation of $\sim \pm 5 \times 10^7\ \mathrm{m\,s^{-1}}$ about $\langle v_\perp \rangle =$

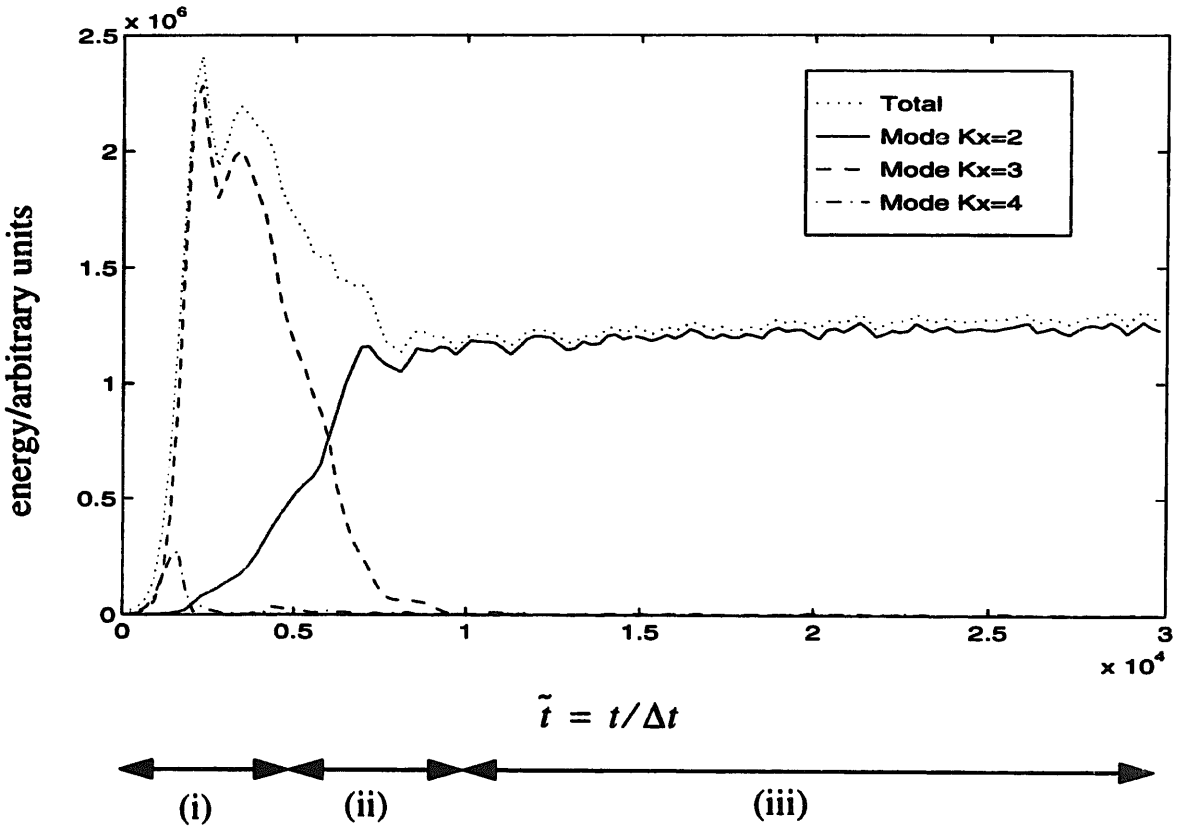

Fig. 8. Magnetic wave energy in wave modes K_x =2–4 during 1-D study 2.

$10^8\,\mathrm{m\,s^{-1}}$, gives an estimated mode 2 trapping period range of $\bar{\tau} = 1380$–$2390\Delta t$ (an estimated primary trapping frequency $\bar{\omega} \approx 0.44\omega_{ce}$, compared with the linearly predicted mode 2 real frequency $\omega_2 \approx 0.22\omega_{ce}$; cf. the corresponding mode 4 frequencies were $\bar{\omega} \approx 0.36\omega_{ce}$ and $\omega_4 \approx 0.4\omega_{ce}$ respectively in study 1, i.e. the two studies do not simply scale to each other). The interval $\tilde{t} > 10000$ is therefore expected to contain roughly ten mode 2 trapping periods for the majority of electrons. Similar calculations show that in the approximately 3000 time step period ($2000 < \tilde{t} < 5000$) during which mode 3 dominates the wave spectrum (see Fig. 8), there are only expected to be about one or two mode 3 trapping periods. Also, the mode 3 wave amplitude varies by almost a factor of two between $\tilde{t} = 2500$ and 5000. For both these reasons, there are not expected to be any significant mode 3 trapping of electrons during the time interval $\tilde{t} < 5000$.

The delay-coordinate plots were produced in the manner described earlier. Fig. 9 shows the positions of the linearly predicted whistler mode cyclotron resonance velocities ($v_{\|res}$) for simulation modes $K_x = 2$–4. The mode 2 resonance velocity is $v_{\|res} \approx -1.1 \times 10^8\,\mathrm{ms^{-1}}$. Hence, any mode 2 trapping effects are expected to be clearly identified in the $v_{\|c} = -10^8\,\mathrm{m\,s^{-1}}$ delay-coordinate plot. We present delay-coordinate plots for the near resonance and off resonance surfaces during $10000 < \tilde{t} < 30000$ only (as expected, trapping effects are seen only in these plots). Far off resonance plots (not shown), as with the corresponding plots in the previous study 1 (see Fig. 6(E) and (F)), show the dominant characteristic frequencies in (untrapped) electron trajectories $v_{\|}(t)$ to be the frequencies of simulation wave modes.

4.2.1. $v_{\|c} = -10^8\,\mathrm{ms^{-1}}$ crossings (near resonant)

Fig. 10(A) $10000 < \tilde{t} < 30000$:- A clear bunching of points around separate characteristic periods is now evident. As in the near resonant crossings during the previous study 1 (see Fig. 6(B)), strong bunching at/around both the electron gyroperiod and

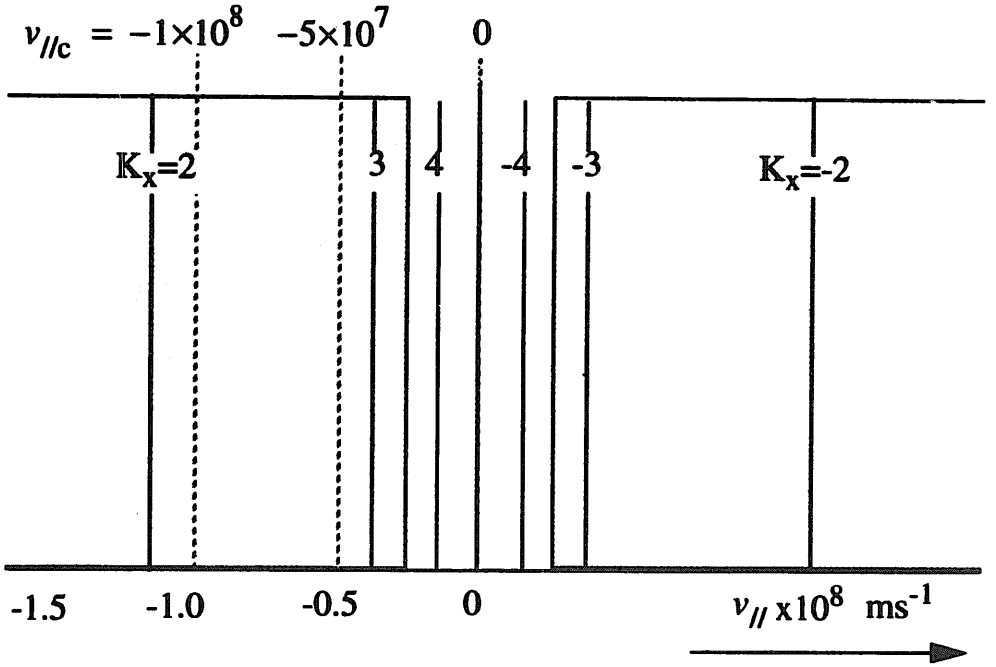

Fig. 9. Phase space picture of the cyclotron resonances and estimated mode 2 trapping region in 1-D study 2. Solid vertical lines represent linearly predicted cyclotron resonance velocities $v_{\|res}$ for the growth modes K_x =2–4; dashed vertical lines represent parallel velocity surfaces chosen for delay-coordinate purposes.

the estimated trapping period is observed. The cluster around $\bar{\tau} = 1690$ is identified as the trapping of a large number of electrons by the dominant wave mode $K_x = 2$ during $\tilde{t} > 10000$. This demonstrates that trapping at/around an estimated trapping period has now been identified in two simulations that are configured, and that evolve, differently.

The trapped population is composed of several identifiable clusters on and off $y = x$, i.e. again suggesting the coupling of at least two strong characteristic frequencies in the phase space motion of trapped electrons (although the trapped cluster geometry is different to that seen near resonance in the previous study 1 results of Fig. 6(B)). The frequency difference between two adjacent clusters (one on $y = x$, one off) is approximately $0.11\omega_{ce}$. As in study 1, secondary trapping resonances are a plausible explanation for this feature. The only simulation wave mode frequency (ω) for which $|\omega - \bar{\omega}|$ is close to the observed frequency difference is that of simulation wave mode 3 (for which $\omega_3 \approx 0.5\omega_{ce}$; c.f. the mode 2 trapping and real trapping frequencies are $\bar{\omega} \approx 0.44\omega_{ce}$ and $\omega_2 \approx 0.22\omega_{ce}$). However, mode 3 contains very little energy relative to the dominant mode 2 during $\tilde{t} > 10000$ (see Fig. 8). Also, the mode 3 cyclotron resonance velocity (the distance from which is a measure of the influence a wave mode exerts on an electron in phase space) is distant from the near resonance surface (see Fig. 9). It therefore, seems unlikely that a coupling of any of the individual simulation wave mode frequencies and the mode 2 trapping frequency can account for the observed pattern in the trapped population.

The distribution of points in the trapped population about the estimated $\bar{\tau}$ and $y = x$ is again asymmetric, there being more points above $y = x$ than below it. Within the estimated range, there are 4022 points above the line $y = x$ and 3529 below it, which is a statistically significant difference (above 8 times $\sqrt{N}$ uncertainties). The Δt_{n+1} of the bunch of asymmetric dots on 10 A is in the vicinity of the minimum, rather than the maximum of the Δt of trapped orbits on the plot, again suggesting that the orbits are not close to the separatrix.

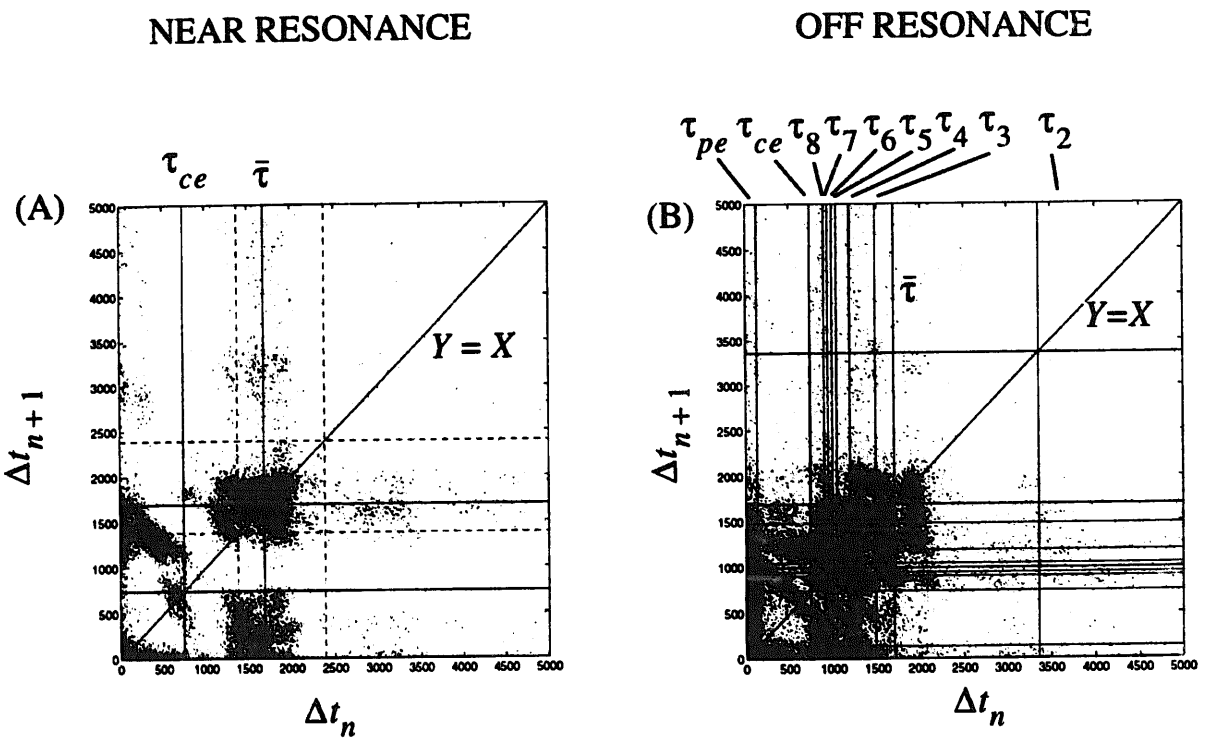

Fig. 10. One-dimensional study 2 delay-coordinate plot showing pairs of crossing periods $(\Delta t_n, \Delta t_{n+1})$ for crossings of (A) $v_{\|c} = -10^8\,\mathrm{m\,s^{-1}}$, (B) $v_{\|c} = -5 \times 10^7\,\mathrm{m\,s^{-1}}$, during $\tilde{t} > 10000$. For clarity purposes, only crossing periods within the range 0–5000 time steps are shown.

Such a clear effect was also observed in study 1. Hence, the earlier discussion (study 1) applies here.

4.2.2. $v_{\|c} = -5 \times 10^7\,\mathrm{m\,s^{-1}}$ *crossings*

Fig. 10(B) $\tilde{t} > 10000$:- There are a variety of characteristic periods of electron motion. All the separate clusters of points at and below the mode 4 wave period (τ_4), both on and off the line $y = x$, coincide with the frequency grid of individual wave modes $K_x = 4, 5, \ldots$. In addition, a population of trapped electrons around $\bar{\tau}$ is evident, with a distribution very similar to that discussed above. Finally, coupling of the strong trapping frequencies and the $K_x = 4, 5, \ldots$ frequency grid leads to the clusters of points above τ_4 and off $y = x$.

5. Conclusions and discussion

The non-linear phase space trapping of electrons in the field of a parallel propagating large amplitude whistler wave has been investigated in detail via two 1-D EM PIC simulations with different scaling. The frequency information in all simulation electrons $v_{\|}(t)$ was analysed by means of delay-coordinate plots, from which we conclude:-

- The primary trapping resonance has been shown to exist under self-consistent conditions. The trapping of a large number of simulation electrons (many thousands) was identified by a cluster of dots on the delay-coordinate plots within the range of the primary trapping period ($\bar{\tau}$) estimated from the observed dominant simulation wave mode amplitude. Trapping was identified in two regions of phase space, near resonance and to a lesser extent off resonance, both of which were expected to lie within the estimated trapping region in phase space.
- The distribution of points on the delay-coordinate plots at/around $\bar{\tau}$ indicated fine structure in phase space structure such that trapped electrons typically undergo phase space motion with at least two strong characteristic frequencies.

- The detailed phase space structure of the trapped electron trajectories shows some evidence of time dependence, with a time evolution towards a lower characteristic oscillation period $\Delta t_{n+1} > \Delta t_n$, but this characteristic Δt_{n+1} is shorter than the maximum period of trapped motion that is observed.

The first of these results concerns the primary trapping resonance, also showing that resonant (trapping) regions of phase space are accessible to particles, and is predicted from non-self-consistent analytical treatments in which a model wave field is prescribed and the trapping process is assumed to be time independent (e.g. [3]). Also, it seems plausible that higher order trapping resonances present in such treatments (when the particle Hamiltonian is taken to higher order in the wave amplitude) may account for the second result. We expect such resonances may be an important consideration at the relatively large wave amplitude representative of the simulations ($B_w/B_0 \sim 0.2$). However, the evidence presented here is somewhat ambiguous, and further work is required in this respect. Although such details are not expected to be important in the magnetospheric problem of VLF emissions ($B_w/B_0 \sim 10^{-6}$–10^{-5} is typical [12]), there may be interesting fusion device based (the non-linear dynamics of particles in a large amplitude wave field are an important consideration in acceleration schemes [2]) and magnetospheric/astrophysical applications (e.g. quasi-parallel bowshock in the earth's magnetosphere, astrophysical shocks). The third result is an evolutionary aspect of the trapping process. The trapping period identified with this evolutionary behaviour is well-defined and is shorter than the maximum period of trapped motion seen; hence it is not consistent with simple Arnold diffusion of trapped electrons towards the separatrix. The delay-coordinate analysis presented here represents the first attempt to directly reconstruct phase space for a self-consistent simulation rather than analytical test particles. Its value as a time series analysis technique has been clearly illustrated in this study. Future simulation and theoretical studies should investigate whether and under what conditions higher order trapping resonances are effective, and the reason(s) for the observed time dependence in the trapping process. Further simulation work in this respect is currently in progress.

Acknowledgements

The authors are grateful to G. Rowlands for helpful discussions. Part of this work was performed whilst P.E. Devine was funded by a PPARC studentship, and S.C. Chapman by a Nuffield Foundation fellowship.

References

[1] Y. Omura, D. Nunn, H. Matsumoto and M.J. Rycroft, A review of observational, theoretical and numerical studies of VLF triggered emissions, J. Atmos. Terr. Phys. 53 (5) (1991) 351–368.

[2] G. Corso and F.B. Rizzato, Stochastic cyclotron dynamics in the interaction of waves and low-energy particles, J. Plasma Phys. 49 (1993) 425–443.

[3] A.J. Lichtenberg and M.A. Lieberman, Regular and Chaotic Dynamics, 2nd Ed. (Springer, New York, 1992).

[4] K.B. Dysthe, Some studies of triggered whistler emissions, J. Geophys. Res. 76 (1971) 6915–6931.

[5] S.C. Chapman and N.W. Watkins, Delay coordinates: A sensitive indicator of nonlinear dynamics in single charged particle motion in magnetic reversals, Annales Geophys. 13 (1995) 836–842.

[6] R. Shaw, The dripping faucet as a model chaotic system, Science Frontier Express Series (Aerial Press, Santa Cruz, 1984).

[7] H. Matsumoto, K. Hashimoto and I. Kimura, Dependence of Coherent Nonlinear Whistler Interaction on Wave Amplitude, J. Geophys. Res. 85 (1980) 644–652.

[8] P.E. Devine, S.C. Chapman and J.W. Eastwood, One- and two-dimensional simulations of whistler-mode waves in an anisotropic plasma, J. Geophys. Res. 100 (1995) 17189–17203.

[9] C.K. Birdsall and S.B. Langdon, Plasma Physics via Computer Simulation (Mc Graw Hill, New York, 1985).

[10] C. Chen, Theory of electron cyclotron resonance laser accelerators, Phys. Rev. A. 10 (1992) 6654–6661.

[11] R. Gendrin, Phase-bunching and other non-linear processes occurring in gyroresonant wave-particle interactions. Astrophys. and Space Sci. 28 (1974) 245–266.

[12] H. Matsumoto, Nonlinear whistler-mode interaction and triggered emissions in the magnetosphere: A Review, in: eds. P.J. Palmadesso and K. Papdopoulos, Wave Instabilities in Space Plasmas (D. Reidel Publishing Company, Dordrecht, 1979) 163–190.